DYNAMIC MODELLING AND EXPERIMENTAL VALIDATION OF A MULTI-BODY UAV

Ahmed Taimah[1], Osama Obeid[1], Eric Lanteigne[1]
[1]*Department of Mechanical Engineering, University of Ottawa, Ottawa, ON, CA*
Email: ataim014@uottawa.ca

ABSTRACT

This paper presents the derivation of a dynamic model for a multi-body LTA (Lighter-than-air) vehicle consisting of a helium filled envelope and a movable gondola. The airship's mathematical model was derived by applying the Boltzmann-Hamel equations, which is used for systems described in terms of quasi-velocities. The derived equations of motion are presented for the simplified case pertaining to only to the airship's lateral motion. The fidelity of the derived model was exhibited by constructing an experimental setup which involved imposing external forces on the physical model and comparing the responses of both the physical and derived models.

Keywords: Dynamic Modelling; Boltzmann-Hamel; Airship; UAV; Multi-body.

MODÉLISATION DYNAMIQUE ET VALIDATION EXPÉRIMENTALE D'UN DRONE MULTICORPS

RÉSUMÉ

Cet article présente la dérivation d'un modèle dynamique pour un véhicule multi-corps plus léger que l'air composé d'une enveloppe remplie d'hélium et d'une nacelle mobile. Le modèle mathématique du dirigeable a été dérivé en appliquant les équations de Boltzmann-Hamel, qui sont utilisées pour les systèmes décrits en termes de quasi-vitesses. Les équations du mouvement sont présentées pour un cas simplifié concernant uniquement les mouvements latéraux du dirigeable. La fidélité du modèle dérivé a été démontrée par la construction d'un montage expérimental : l'application de forces externes sur le système physique a permis de comparer les réponses du système physique et du modèle dérivé.

Mots-clés : Modélisation dynamique ; Boltzmann-Hamel ; Dirigeable ; Drone ; Multi-corps..

1. INTRODUCTION

Unmanned Aerial Vehicles (UAVs), namely airships, have been widely adopted in recent years due to their ability to perform a variety of automated tasks. A key advantage of LTA aircraft is their ability to remain airborne for extended periods of time without requiring frequent refueling, making them ideal for tasks that require long-duration flights, such as aerial surveillance and monitoring. Another advantage of LTA UAVs is their ability to carry heavy payloads over long distances. Additionally, LTA UAVs can be used as a platform for communication equipment, such as radios and cellular networks, which is useful in areas where traditional communication infrastructure may be lacking. To optimize the mentioned benefits regarding UAVs, it is essential to derive a vehicle dynamic model that blends theoretical principles with experimental data to precisely depict the system's dynamics.

The two primary approaches of dynamic modelling in classical mechanics are the Lagrangian and Newton-Euler mechanics. The Lagrangian approach utilizes the difference between the system's kinetic energies, while the Newton-Euler approach involves applying Euler's laws of rigid body dynamics to the system's translational and rotational dynamics [1]. Due to the resurgence of LTA airships in recent years, vehicles modelled using the Newton-Euler approach [2–4] and the Lagrangian approach [5, 6] have been thoroughly studied and aided in the advancement of airship modelling. Numerous dynamic models have been developed for single-body conventional airships and can be found in the literature. However, the literature contains only a limited number of dynamic models for multi-body unmanned airships. One of the primary obstacles encountered when modelling multi-body airships is accommodating for non-holonomic constraints, which are non-integrable constraints on the motion and/or non-integrable quasi-velocities which require the use of Lagrange multipliers when using Lagrange's equations [7]. The Boltzmann-Hamel equations can be directly applied to system with non-integrable constraints or quasi-velocities [8].

The airship presented in this investigation is a multi-body consisting of a helium filled envelope and a reconfigurable gondola housing the motors for actuation of the airship. The gondola slides on a rail attached to the envelope, which allows it to control the pitch attitude of the airship as desired. The derived model will be used to train a controller utilized to govern the airship's lateral behaviour.

This paper is presented as follows. The individual terms of the Boltzmann-Hamel equations are derived, and the airship's equations of motion are then developed. Then, an experimental setup for the model's validation is described. Finally, a conclusion of the results and the effectiveness of the model are discussed.

2. MULTI-BODY MODELLING

To model the multi-body LTA aircraft, some assumptions must be stated beforehand.

- The airship's center of volume (CV) and center of buoyancy (CB) are assumed to be coincident.
- The airship's added mass and inertia due to the large volume of air displaced are considered.
- The airship's body is assumed to be rigid with a constant volume, therefore any aeroelastic effects will be neglected.

2.1. Kinematics

The prototype is composed of two bodies, the blimp and the gondola. The blimp consists of an envelope, helium, rail and fins. The blimp's mass is denoted by m_1, the gondola's mass is denoted by m_2, and the total mass which is the summation of both m_1 and m_2, is denoted by m_t. Often in multi-body systems, the body axis is located at the centre of volume CV, which is static when constant volume is assumed, as opposed to a vehicle's total center of gravity CG, which position depends on the location of each body present in a

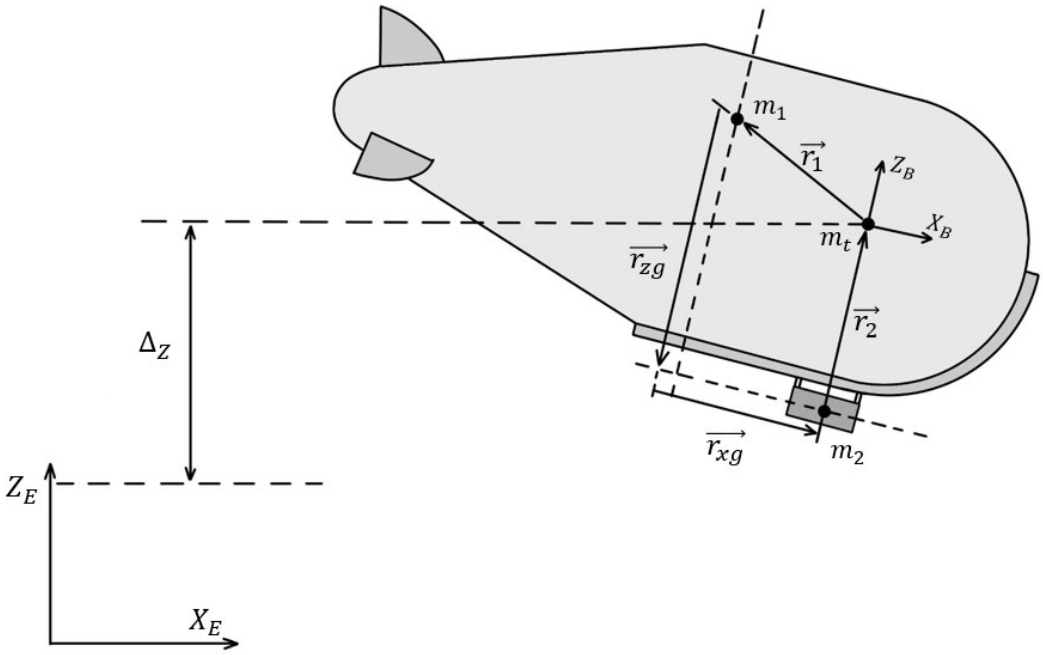

Fig. 1. Airship Coordinate System

multi-body. This paper adapts a different approach for the body axis center location, reason being is that this research concerns the lateral motion of a multi-body UAV. Since the gondola is only used to govern the longitudinal behaviour of the airship, the gondola's position will remain constant. Maintaining the gondola's CG_g position throughout an experiment would cause the vehicle's total CG_v to be fixed throughout flight, deeming the CG_v an appropriate location for the body frame's axis origin. As seen in Figure 1, the body frame is attached to the multi-body's m_t centre of gravity rather than the center of volume CV. Both the body reference frame $[X_b \ Y_b \ Z_b]$ and the inertial reference frame $[X_i \ Y_i \ Z_i]$ adhere to a North-West-Up directional convention. The generalized coordinates expressed in the inertial frame are:

$$\vec{\mathbf{q}} = [x \ y \ z \ \phi \ \theta \ \psi \ Sg]^T \tag{1}$$

The generalized coordinates $(\phi, \ \theta, \ \psi)$ seen in (1) are known as Euler angles, namely roll ϕ, pitch θ, and yaw ψ. Euler angles can be used to describe any of the airship's body rotations relative to an either inertial or body frame of reference [9]. A rotation matrix can be developed to transform coordinates from the body frame to the inertial frame, by setting up intermediate reference frames. Information on the rotation matrices' development can be found in Appendix A. The resulting transformation matrices are:

$$\mathbf{{}^{E}_{B}R_1} = \begin{bmatrix} cos(\psi)cos(\theta) & cos(\psi)sin(\phi)sin(\theta) - cos(\phi)sin(\psi) & sin(\phi)sin(\psi) + cos(\phi)cos(\psi)sin(\theta) \\ cos(\theta)sin(\psi) & cos(\phi)cos(\psi) + sin(\phi)sin(\psi)sin(\theta) & cos(\phi)sin(\psi)sin(\theta) - cos(\psi)sin(\theta) \\ -sin(\theta) & cos(\theta)sin(\phi) & cos(\phi)cos(\theta) \end{bmatrix} \tag{2}$$

$$\mathbf{R_2} = \begin{bmatrix} 1 & 0 & -sin(\theta) \\ 0 & cos(\phi) & sin(\phi)cos(\theta) \\ 0 & -sin(\phi) & cos(\phi)cos(\theta) \end{bmatrix} \tag{3}$$

Combining (4), the kinematic loop closure equation, and (5), the summation of moments, yields a relation that associates both the blimp and the gondola's centers of gravity to the airship's center of gravity CG_v, in the inertial frame. $\vec{r_1}$ is the vector from the vehicle's CG to the blimp's CG, and $\vec{r_2}$ is the vector from the vehicle's CG to the gondola's CG. $\vec{r_{zg}}$ is the vector from the blimp's CG to the gondola's CG in the Z direction, and $\vec{r_{xg}}$ is the vector from $\vec{r_{zg}}$ to the gondola, in the X direction, thus completing the loop.

$$\vec{\mathbf{r_1}} + \vec{\mathbf{r_{zg}}} + \vec{\mathbf{r_{xg}}} = \vec{\mathbf{r_2}} \tag{4}$$

$$\vec{\mathbf{r_1}} m_1 + \vec{\mathbf{r_2}} m_2 = 0 \tag{5}$$

Since the relationship between the different $CG's$ and CV is in the inertial frame, R_1 must be multiplied into the vectors, thus yielding:

$$\begin{bmatrix} r_{1x} \\ r_{1y} \\ r_{1z} \end{bmatrix} + \mathbf{R_1} \begin{bmatrix} 0 \\ 0 \\ -z_g \end{bmatrix} + \mathbf{R_1} \begin{bmatrix} x_g \\ 0 \\ 0 \end{bmatrix} = \begin{bmatrix} r_{2x} \\ r_{2y} \\ r_{2z} \end{bmatrix} \tag{6}$$

$$\vec{\mathbf{r_{zg}}} = \mathbf{R_1} \begin{bmatrix} 0 & 0 & -z_g \end{bmatrix}^T = z_g \begin{bmatrix} -(sin(\phi)sin(\psi) + cos(\psi)sin(\theta)cos(\phi)) \\ -(cos(\phi)sin(\psi)sin(\theta) - cos(\psi)sin(\phi)) \\ -cos(\phi)cos(\theta) \end{bmatrix} \tag{7}$$

$$\vec{\mathbf{r_{xg}}} = \mathbf{R_1} \begin{bmatrix} x_g & 0 & 0 \end{bmatrix}^T = x_g \begin{bmatrix} cos(\psi)cos(\theta) \\ cos(\theta)sin(\psi) \\ -sin(\theta) \end{bmatrix} \tag{8}$$

Substituting equations (7) and (8) into (4) and solving equations (4) and (5) simultaneously produces the following results:

$$r_{1x} = m_2 \frac{a_x}{(m_1 + m_2)} \tag{9}$$

$$r_{1y} = -m_2 \frac{a_y}{(m_1 + m_2)} \tag{10}$$

$$r_{1z} = m_2 \frac{a_z}{(m_1 + m_2)} \tag{11}$$

$$r_{2x} = -m_1 \frac{a_x}{(m_1 + m_2)} \tag{12}$$

$$r_{2y} = m_1 \frac{a_y}{(m_1 + m_2)} \tag{13}$$

$$r_{2z} = -m_1 \frac{a_z}{(m_1 + m_2)} \tag{14}$$

where the coefficients a are a function of the position of both the envelope and gondola's CG , and can be found in full in Appendix B.

The blimp has a rail where the gondola is mounted onto, which consists of a straight rail segment and a curved rail segment, as observed in figure 2.

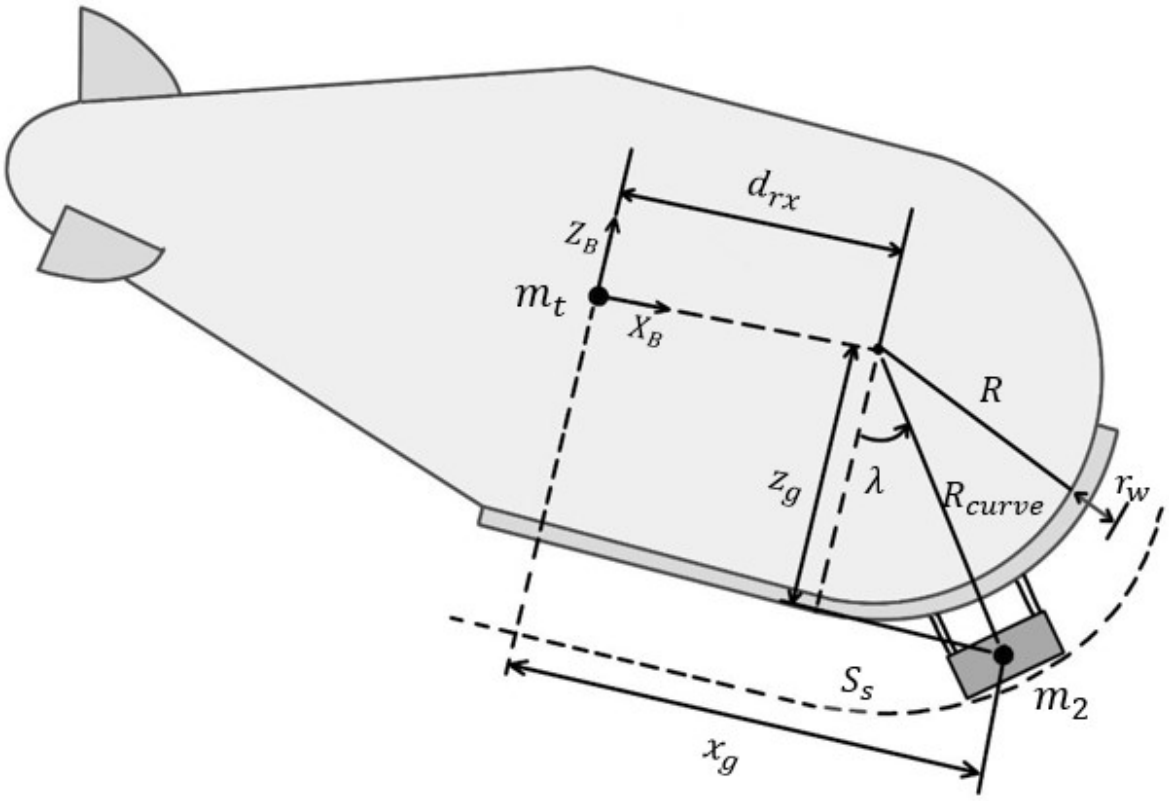

Fig. 2. Gondola on Curved Rail

The gondola's position can defined by two variables, x_g and z_g, that are both functions of the gondola's position on the rail, S_s.

$$x_g = \begin{cases} S_s & \text{for, } -0.6 \geq S_s \geq 0.3 \\ d_{rx} + sin\left(\dfrac{S_s - d_{rx}}{R_{curve}}\right) R_{curve} & \text{for, } 0.3 < S_s \leq 2.14 \end{cases} \tag{15}$$

$$z_g = \begin{cases} l & \text{for, } -0.6 \geq S_s \geq 0.3 \\ \sqrt{(R_{curve})^2 - \left(sin\left(\dfrac{S_s - d_{rx}}{R_{curve}}\right) R_{curve}\right)^2} & \text{for, } 0.3 < S_s \leq 2.14 \end{cases} \tag{16}$$

Equation (15) shows that the value of x_g is equal to the position of the gondola on the rail, S_s, until the gondola is on the curved section, where x_g is defined by a function that accounts for the curvature of the rail. Similarly, equation (16) displays how z_g is equal to l, the vertical distance between the airship's CG_v and the gondola's CG_g, until the gondola is on the curved section of the rail, where z_g is also defined by a function that accounts for the curvature of the rail. Table 1 contains the other variables seen in Figure 2.

Symbol	Parameter	Value
d_{rx}	Distance between the center of the circumference and the origin of the body frame, along the x axis	0.3 m
l	Distance between the total CG and the gondola CG, along the z axis	0.94 m
R	Radius of the curve	0.9 m
r_w	Rail thickness + added material	0.045 m

Table 1. Gondola-Rail Parameters

2.2. Mass Matrix

The blimp's mass m_1 described in equation (17) is the sum of the envelope, helium, rail and fins' masses.

$$m_1 = m_{envelope} + m_{helium} + m_{rail} + m_{fins} \tag{17}$$

The gondola's total mass m_2, consists of the gondola, which includes all onboard electronics and thrusters, and the added counterweight $m_{addedCW}$ which is used to balance the bouyancy force caused by the helium. Therefore this mass value will vary depending on how much added mass is required to maintain the blimp in a buoyant state.

$$m_2 = m_{gondola} + m_{addedCW} \tag{18}$$

The airship's total mass is given by:

$$m_t = m_1 + m_2 \tag{19}$$

The 6x6 mass matrix for the airship can be expressed:

$$\mathbf{M} = \begin{bmatrix} \mathbf{M_a} & 0 \\ 0 & \mathbf{J_a} \end{bmatrix} \tag{20}$$

where $\mathbf{M_a}$ and $\mathbf{J_a}$ are both 3x3 matrices.

Any fluid surrounding a body in motion is to be displaced, in that body's direction of motion [10]. For airships, the resisting air's mass and inertia can be accounted for by adding virtual, or added, mass and inertia terms, to account for this phenomenon.

$$\mathbf{M_a} = \begin{bmatrix} m_x & 0 & 0 \\ 0 & m_y & 0 \\ 0 & 0 & m_z \end{bmatrix} \tag{21}$$

$$\mathbf{J_a} = \begin{bmatrix} J_x & 0 & J_{xz} \\ 0 & J_y & 0 \\ J_{xz} & 0 & J_z \end{bmatrix} \tag{22}$$

$$m_x = (1 + k_1)(m_1 + m_2) \tag{23}$$

$$m_y = m_z = (1 + k_2)(m_1 + m_2) \tag{24}$$

$$J_x = I_{B_x} + I_{G_x} \tag{25}$$

$$J_y = (1+k')(I_{B_y} + I_{G_y}) \tag{26}$$

$$J_z = (1+k')(I_{B_z} + I_{G_z}) \tag{27}$$

$$J_{xz} = (I_{B_{xz}} + I_{G_{xz}}) \tag{28}$$

$\mathbf{M_a}$ and $\mathbf{J_a}$ are mass and inertia matrices that account for the system's total mass and inertia in addition to the calculated added mass and inertia, respectively. In rectilinear motion ,the effect of added mass and inertia is equivalent to k times the mass of the displaced fluid [11]. These added terms have been calculated by utilizing Lamb's coefficients, that estimate the added mass to an ellipsoid in the axial k_1, transverse k_2, and rotational k' directions of motion.

$$\mathbf{M} = \begin{bmatrix} m_x & 0 & 0 & 0 & 0 & 0 \\ 0 & m_y & 0 & 0 & 0 & 0 \\ 0 & 0 & m_z & 0 & 0 & 0 \\ 0 & 0 & 0 & J_x & 0 & J_{xz} \\ 0 & 0 & 0 & 0 & J_y & 0 \\ 0 & 0 & 0 & J_{xz} & 0 & J_z \end{bmatrix} \tag{29}$$

Symbol	Parameter	Value	Units
m_1	Blimp's Mass	2.66	kg
m_2	Gondola's Mass	3.3	kg
k_1	Lamb's Inertia Ratio in the Axial Direction	0.1664	–
k_2	Lamb's Inertia Ratio in the Lateral Direction	0.69	–
k'	Lamb's Inertia Ratio about the Vertical Axis	0.3364	–
I_{B_x}	Blimp's Moment of Inertia about the X Axis	0.87	$kg\,m^2$
I_{B_y}	Blimp's Moment of Inertia about the Y Axis	3.72	$kg\,m^2$
I_{B_z}	Blimp's Moment of Inertia about the Z Axis	3.72	$kg\,m^2$
I_{G_x}	Gondola's Moment of Inertia about the X Axis	0.136	$kg\,m^2$
I_{G_y}	Gondola's Moment of Inertia about the Y Axis	0.15	$kg\,m^2$
I_{G_z}	Gondola's Moment of Inertia about the Z Axis	0.15	$kg\,m^2$
$I_{B_{xz}}$	Blimp's Moment of Inertia about the X-Z Plane	0	$kg\,m^2$
$I_{G_{xz}}$	Gondola's Moment of Inertia about the X-Z Plane	0	$kg\,m^2$

Table 2. Mass Matrix Parameters

2.3. Dynamics

2.3.1. Kinetic Energy

The airship's total Kinetic Energy $T(\vec{\mathbf{q}}, \vec{\mathbf{q}}, t)$ can be defined as:

$$T = T_1 + T_2 + T_a \tag{30}$$

Kinetic energy requires true velocities that are based on the generalized coordinates that represent the vehicle's position relative to an inertial frame [12]. Therefore, body-fixed velocities such as (p,q,r) are not acceptable. The three kinetic energy sources to be considered are the translational kinetic energy $T = \frac{1}{2}m\vec{v}^2$

from the blimp and gondola's CG's to the vehicle's CG_v, the rotational kinetic energy $T = \frac{1}{2}I\vec{\omega}^2$ from the blimp CG to the vehicle's CG_v, and finally the total (translational and rotational) kinetic energy from the vehicle's CG_v, which includes the added mass and inertia, to the earth frame.

$$T_1 = \frac{1}{2}\dot{\vec{\mathbf{r}}}_{\mathbf{1}}^{\,T} m_1 \dot{\vec{\mathbf{r}}}_{\mathbf{1}} + \frac{1}{2} I_1 \vec{\omega}^2 \tag{31}$$

where I_1 is a 3x3 matrix consisting of the envelope's moments of inertia, $\vec{\omega}$ is a vector of the angular velocities, and T_1 is the kinetic energy due to the relative translational and rotational motion between m_1 and the vehicle's CG_v.

$$T_2 = \frac{1}{2}\dot{\vec{\mathbf{r}}}_{\mathbf{2}}^{\,T} m_2 \dot{\vec{\mathbf{r}}}_{\mathbf{2}} + \frac{1}{2} I_2 \vec{\omega}^2 \tag{32}$$

T_2 is the kinetic energy due to the relative motion between m_2 and the vehicle's CG_v. T_a is the kinetic energy due to the velocity contribution of m_1, m_2 and the added mass relative to the inertial frame.

$$T_a = \frac{1}{2}\vec{\mathbf{V}}^T \mathbf{M} \vec{\mathbf{V}} \tag{33}$$

The velocity contributions with respect to the inertial frame for m_1, m_2 and the added mass are included in T_a, by utilizing the mass matrix M to account for them, by adding 1 to the Lamb coefficients, as can be seen in equations (23) - (27). $\vec{\mathbf{V}}$ is a velocity matrix that includes the linear velocities $\vec{\mathbf{v}} = [\dot{x} \;\; \dot{y} \;\; \dot{z}]^T$ and the angular velocities $\vec{\omega} = [\dot{\phi} \;\; \dot{\theta} \;\; \dot{\psi}]^T$.

2.3.2. Potential Energy

The airship's total potential energy U is the sum of the blimp and gondola's potential energies, denoted by U_1 and U_2, respectively.

$$U = U_1 + U_2 \tag{34}$$

U_1 is the potential energy of the blimp's mass m_1 less the mass of the displaced air m_{air}.

$$U_1 = g(m_1 - m_{air})(z - r_{1z}) \tag{35}$$

The blimp is designed to operate at a low altitude of approximately 122 meters [13]. To calculate the air pressure and mass, certain assumptions were made, including an atmospheric temperature of $20°C$, a decrease in air density $\Delta\rho = -1.164e^{-4}\, kg/m^4$, and that the airships volume V remains constant [8]. For a given altitude z, the air's density can be estimated by:

$$\rho_{air} = \rho_{ref} - \Delta\rho\Delta z \tag{36}$$

where ρ_{ref} is the air density at the reference altitude z_{ref}. At the reference altitude, $m_{air} = \rho_{reF}V = m_t$, and a relation describing the air's mass as relative to the vehicle's mass can be expressed as:

$$m_{air} = \frac{\rho_{ref} - \Delta\rho\Delta z}{\rho_{ref} - \Delta\rho z_{ref}} m_t \tag{37}$$

The gondola's potential energy can be computed as:

$$U_2 = g m_2 (z - r_{2z}) \tag{38}$$

Finally, the system's total potential energy is

$$U = g\left((m_1 - m_{air})(z - r_{1z}) + m_2(z - r_{2z})\right) \tag{39}$$

2.4. Quasi-Velocities

Typically in UAVs, the angular velocities are represented by body frame velocities ω, rather than rate of change of Euler angles $(\dot{\phi}, \dot{\theta}, \dot{\psi})$ [8]. These quasi-velocities *us* are non-integrable, such that if they were, they would be true velocities $\dot{q}s$.

The transformation relating *us* and $\dot{q}s$ in an unconstrained system [12] can be seen in Equation (40)

$$\mathbf{u_j} = \sum_{i=1}^{n} \Psi_{ji}(q,t)\dot{q}_i \quad (j = 1,...,n) \tag{40}$$

where n is the number of degrees of freedom in the system. Ψ_{ji} is a $(n \times n)$ matrix that transforms the derivatives of the generalized coordinates into the quasi-velocities. Furthermore, $\Phi_{ij} = \Psi_{ji}^{-1}$, resulting in the inverse relationship:

$$\dot{\mathbf{q}}_\mathbf{i} = \sum_{j=1}^{n} \Phi_{ij}(q,t)u_j \quad (i = 1,...,n) \tag{41}$$

A detailed derivation of the quasi-velocities can be found in Appendix C

The matrix transforming true velocities to quasi-velocities can now is defined as:

$$\Psi_{ji}(q,t) = \begin{bmatrix} cos(q_6)cos(q_5) & sin(q_6)cos(q_5) & -sin(q_5) & 0 & 0 & 0 & 0 \\ b_1 & b_2 & cos(q_5)sin(q_4) & 0 & 0 & 0 & 0 \\ b_3 & b_4 & cos(q_5)cos(q_4) & 0 & 0 & 0 & 0 \\ 0 & 0 & 0 & 1 & 0 & -sin(q_5) & 0 \\ 0 & 0 & 0 & 0 & cos(q_4) & cos(q_5)sin(q_4) & 0 \\ 0 & 0 & 0 & 0 & -sin(q_4) & cos(q_5)cos(q_4) & 0 \\ 0 & 0 & 0 & 0 & 0 & 0 & 1 \end{bmatrix} \tag{42}$$

$$b_1 = cos(q_6)sin(q_5)sin(q_4) - sin(q_6)cos(q_4) \tag{43}$$

$$b_2 = sin(q_6)sin(q_5)sin(q_4) + cos(q_6)cos(q_4) \tag{44}$$

$$b_3 = cos(q_6)sin(q_5)cos(q_4) + sin(q_6)sin(q_4) \tag{45}$$

$$b_4 = sin(q_6)sin(q_5)cos(q_4) - cos(q_6)sin(q_4) \tag{46}$$

2.5. Aerodynamics

The aerodynamic terms used for this model have been derived from numerical simulations [14].

2.6. Boltzmann-Hamel

The dynamics of a system can be defined by the Lagrangian:

$$L = T - U \tag{47}$$

which utilizes the system's energies rather than its forces [1]. When dealing with a system that involves quasi-velocities, applying the Lagrangian approach in a straightforward manner will not yield accurate equations, therefore the Lagrangian must be redefined as:

$$L^*(q,u,t) = L(q,\dot{q},t) \tag{48}$$

As previously stated, the dynamic model for this system concerns the lateral behaviour of the multi-body, and for that the gondola's motion will be restricted. To develop a lateral model, θ was set to zero, and the value of z was held constant at the reference altitude aforementioned. This results in a model that captures the airship's lateral dynamics while maintaining a 3D mathematical model. Restraining the gondola's motion overcomes the non-holonomic nature of the multi-body. allowing for the use of the generalized Boltzmann-Hamel equation:

$$\frac{d}{dt}\left(\frac{\delta L}{\delta u_r}\right) - \sum_{i=1}^{n}\left(\frac{\delta L}{\delta \theta_r}\right) + \sum_{j=1}^{n}\sum_{l=1}^{n}\frac{\delta L}{\delta u_j}\gamma_{rl}^{j}u_l = Q_r \quad (r = 1,...,n) \tag{49}$$

where n is the number of degrees of freedom, θ_r are the generelized coordinates, and γ_{rl}^{j} is the hamel coefficient defined by:

$$\gamma_{rl}^{j}(q) = -\gamma_{lr}^{j} = \sum_{i=1}^{n}\sum_{k=1}^{n}\left(\frac{\delta \Psi_{ji}}{\delta q_k} - \frac{\delta \Psi_{jk}}{\delta q_i}\right) \tag{50}$$

The results of the Boltmann-Hamel equation are lengthy and not presented, but were obtained by solving for the system's kinematics $\vec{r}_1$ and $\vec{r}_2$, computing the mass matrix M, and then calculating the system's dynamics. Once that has been achieved, the equations were simplified for the lateral case, and the Lagrangian was expressed in quasi-velocities. Finally, the terms in the Boltzmann-Hamel equations were computed and summed, and then solved for the lateral set of equations of motion $\ddot{x}$, $\ddot{y}$, $\ddot{\phi}$ and $\ddot{\psi}$.

3. EXPERIMENTAL VALIDATION

To validate the derived dynamic model, an experiment was carried out indoors. The experiment is performed in open loop with no control actuation. Forces are applied to the multi-body by hand using a load cell. The load cell measures the magnitude of the applied force and stores it. A description of the load cell will be given later. The trajectory of the multi-body is then traced using OptiTrack motion capture system. The motion capture system consists of 20 synchronized cameras that locate the position of traced bodies using triangulation. Triangulation requires attaching reflectors on traced bodies. Over 20 reflectors were attached to the blimp while the gondola had 10 reflectors (Figure3).

Fig. 3. Multi-body is depicted inside the workspace during experiment set up.

Knowing the magnitude of the applied forces as a function of time and the initial conditions of the multi-body allow simulating the experiment using the model derived earlier. Trajectory produced by simulation is then compared with the experimental data acquired by the motion capture system.

3.1. Experiment Layout

The envelope was filled with helium which resulted in buoyancy force that lifted the multi-body. To maintain a fixed altitude of the multi-body, calibration weights were added manually on top of the gondola. Forces were applied to the blimp for 1.2 seconds. The forces were applied away from CG of the blimp which yielded a yawing moment about z-axis. Owing to workspace limitations, the duration of the experiment was only 5 seconds.

3.2. Description of Load Cell Device

In order to simulate the experiment described earlier, it is necessary to record the sequence of applied forces. The time history of the applied force was measured using a load cell [15]. The load cell is powered by a 9V battery and produces an analog signal between 0.5-5V. For reading and storing the output signal, the load cell was connected to Arduino Mega 2560. Moreover, the load cell requires a mount in order to be conveniently used in an experiment. A hinged arm was designed to convey the applied force to the load cell while ensuring that the friction at the hinge is minimal. The mount, Arduino, and load cell are depicted in Figure 4.

After assembling the load cell device, calibration was performed by placing calibration weights on the load cell and reading the output voltage. Repeating this process using multiple weights yields a relationship between voltage and force which can be represented faithfully with a linear fit (Figure4).

During the experiment, data was stored on Arduino's EEPROM by first setting all bytes to zero followed by storing the signal received from the load cell (through designated analogue pins). Finally, data was retrieved from Arduino and converted from bytes to physical values, *i.e.,* voltage.

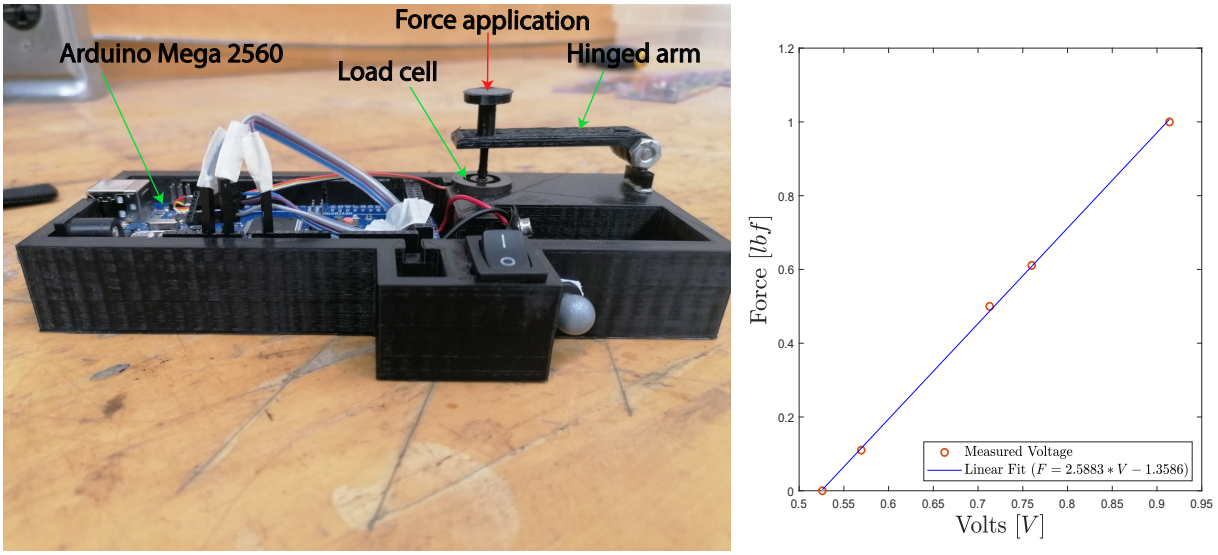

Fig. 4. Load cell device used to measure the applied force (left). Load cell calibration, showing a linear relationship between voltage and force (right)

3.3. Results and Discussion

The experiment conducted to evaluate the veracity of the derived dynamic airship model comprised of an external force applied onto the airship. The initial position of the multi-body was $-0.86\,m$ and $0.69\,m$ in the axial and lateral directions, respectively. The applied forces are depicted in Figure 5.

$$E = ||(P_B)_{Simulation} - (P_B)_{Experiment}||^2 + ||(P_G)_{Simulation} - (P_G)_{Experiment}||^2 \tag{51}$$

$$E_{RMS} = \sqrt{\overline{E}} \tag{52}$$

where P_B and P_G are, respectively, the blimp and gondola's positions, E_{RMS} is the root mean squared error, and $\overline{E}$ is the mean squared error. Examining Figure 5, it is observed that there is a discrepancy in the gondola's trajectory. The position error between the experiment and simulation is calculated using (52), and was found to be $0.23\,m$. This error represents the total distance discrepancy between the simulation output and experimental data. This disparity of positional accuracy can be attested to the estimated inertial values, particularly the added mass and inertia terms. Nonetheless, the behaviour of the simulated model is consistent with the empirical results. To improve the model's accuracy, system identification can be applied to the physical prototype, to acquire the airship's added mass and inertia values.

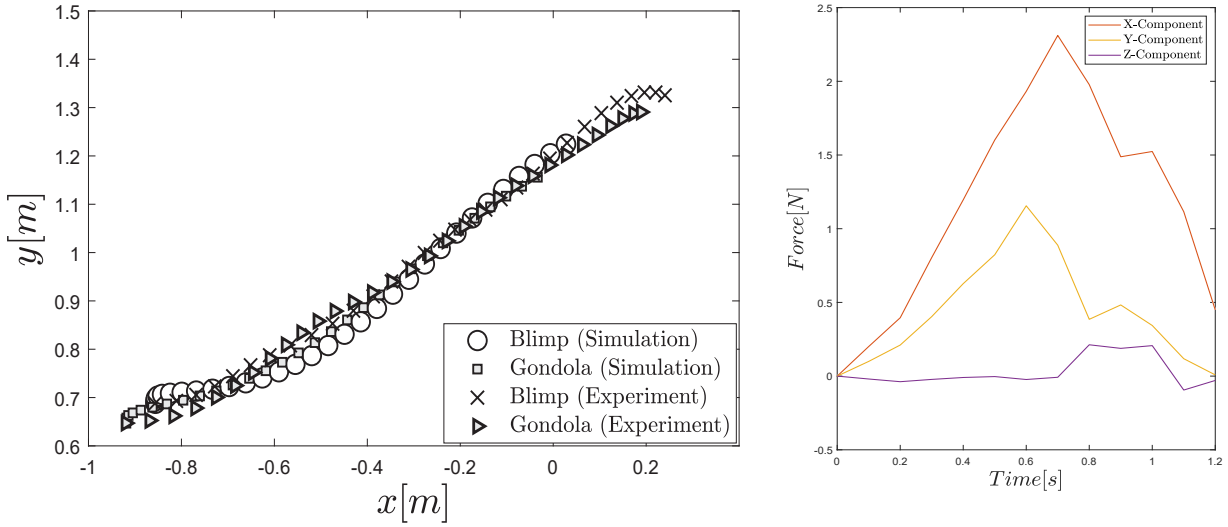

Fig. 5. Position of blimp and gondola based on the experiment and simulation (left). Components of applied forces (right).

4. CONCLUSIONS

The focus of this paper was the derivation of a dynamic model for the lateral motion of a multi-body unmanned airship, achieved through the use of Boltzmann-Hamel equations. The presented model was then verified through experimental validation, which yielded promising results that can be improved by using more accurate parameters acquired by system identification. Although the paper only presents a simplified version of the model, the approach described can be readily implemented to the complete dynamic model of the airship or any other multi-body vehicle.

REFERENCES

1. Pila, A.W. *Introduction to lagrangian dynamics*. Springer, 2019.
2. Fossen, T.I. "Guidance and control of ocean vehicles." *University of Trondheim, Norway, Printed by John Wiley & Sons, Chichester, England, ISBN: 0 471 94113 1, Doctors Thesis*, 1999.
3. Lanteigne, E., Alsayed, A., Robillard, D. and Recoskie, S.G. "Modeling and control of an unmanned airship with sliding ballast." *Journal of Intelligent & Robotic Systems*, Vol. 88, pp. 285–297, 2017.
4. Frye, M.T., Gammon, S.M. and Qian, C. "The 6-dof dynamic model and simulation of the tri-turbofan remote-controlled airship." In "2007 American Control Conference," pp. 816–821. doi:10.1109/ACC.2007.4283087, 2007.
5. Gomes, S.B. *An Investigation of the Flight Dynamics of Airships with Application to the YEZ-2A*. Ph.D. thesis, Cranfield Institute of Technology, 1990.
6. Cook, M. "The linearised small perturbation equations of motion for an airship." Tech. Rep., 1990.
7. Cameron, J. and Book, W. "Modeling mechanisms with nonholonomic joints using the botzmann-hamel equations." *I. J. Robotic Res.*, Vol. 16, pp. 47–59. doi:10.1177/027836499701600104, 02 1997.
8. Lanteigne, E. and O'Reilly, J. "Multibody dynamic modeling and control of an unmanned aerial vehicle under non-holonomic constraints." In "2020 International Conference on Unmanned Aircraft Systems (ICUAS)," pp. 316–321. doi:10.1109/ICUAS48674.2020.9213950, 2020.
9. Weisstein, E.W. "Euler angles." *https://mathworld. wolfram. com/*, 2009.
10. Khoury, G.A. *Airship technology*, Vol. 10. Cambridge university press, 2012.
11. Lamb, H. "The inertia coefficients of an ellipsoid moving in fluid." *Advisory Committee for Aeronautics, Reports and Memoranda No. 623, London, UK*, 1918.
12. Greenwood, D.T. *Frontmatter*, pp. i–iv. Cambridge University Press, 2003.
13. GovernmentofCanada. "901.25 (1).", November 2009.
14. Obeid, O. and Lanteigne, E. "Dynamic modelling of multi-body unmanned airship with a slung-payload." In "2022 IEEE International Symposium on Robotic and Sensors Environments (ROSE)," pp. 1–7. doi: 10.1109/ROSE56499.2022.9977433, 2022.
15. TE Connectivity. *FX29 Compact Compression Load Cell*, 2022.

APPENDIX

A. DERIVING THE TRANSFORMATION MATRICES

First, a rota tion about the x-axis with an angle of ϕ occurs, shifting the y and z axes from the body axis frame to a new axis, intermediate frame 1, and is denoted by R_x. Then, there is a rotation of θ about the y-axis, traversing the current axis into intermediate frame 2, denoted by R_y. Finally, denoted by R_z, there is a rotation of ψ about the z-axis, shifting the axis system into its final axis, the inertial frame.

$$ {}^{1}_{B}R_x(\phi) = \begin{bmatrix} 1 & 0 & 0 \\ 0 & cos(\phi) & -sin(\phi) \\ 0 & sin(\phi) & cos(\phi) \end{bmatrix} \tag{53} $$

$$ {}^{2}_{1}R_y(\theta) = \begin{bmatrix} cos(\theta) & 0 & sin(\theta) \\ 0 & 1 & 0 \\ -sin(\theta) & 0 & cos(\theta) \end{bmatrix} \tag{54} $$

$$ {}^{E}_{2}R_z(\psi) = \begin{bmatrix} cos(\psi) & -sin(\psi) & 0 \\ sin(\psi) & cos(\psi) & 0 \\ 0 & 0 & 1 \end{bmatrix} \tag{55} $$

To compute the rotation matrix R_1, the product of all the angle rotations must be computed, such that:

$$ {}^{E}_{B}R_1 = {}^{E}_{2}R_z(\psi){}^{2}_{1}R_y(\theta){}^{1}_{B}R_x(\phi) \tag{56} $$

Solving 56,

$$ {}^{E}_{B}R_1 = \begin{bmatrix} cos(\psi)cos(\theta) & cos(\psi)sin(\phi)sin(\theta) - cos(\phi)sin(\psi) & sin(\phi)sin(\psi) + cos(\phi)cos(\psi)sin(\theta) \\ cos(\theta)sin(\psi) & cos(\phi)cos(\psi) + sin(\phi)sin(\psi)sin(\theta) & cos(\phi)sin(\psi)sin(\theta) - cos(\psi)sin(\theta) \\ -sin(\theta) & cos(\theta)sin(\phi) & cos(\phi)cos(\theta) \end{bmatrix} \tag{57} $$

Equation (57) can be used to convert coordinates from the body to the earth reference frame, and its inverse R_1^{-1} can be used to convert from the earth to the body reference frame.

The matrix R_1 deals with converting coordinates from the body frame to coordinates in the earth frame. In order to convert angular velocities in the inertial frame $\begin{bmatrix} \dot{\phi} & \dot{\theta} & \dot{\psi} \end{bmatrix}^T$ to angular velocities in the body frame $\begin{bmatrix} p & q & r \end{bmatrix}^T$, a rotation matrix R_2 is introduced.

$$ \begin{bmatrix} p \\ q \\ r \end{bmatrix} = R_2 \begin{bmatrix} \dot{\phi} \\ \dot{\theta} \\ \dot{\psi} \end{bmatrix} \tag{58} $$

From deriving R_1, R_x, R_y and R_z have already been calculated. For $R_x(\phi)$, the only rotation occurs in $\dot{\phi}$, such that

$$ {}^{1}_{B}\overline{\omega}^{B} = {}^{1}_{B}\overline{\omega}^{1} = \begin{bmatrix} \dot{\phi} \\ 0 \\ 0 \end{bmatrix} \tag{59} $$

Similarly,

$$ {}^{2}_{1}\overline{\omega}^{2} = {}^{2}_{1}\overline{\omega}^{1} = \begin{bmatrix} 0 \\ \dot{\theta} \\ 0 \end{bmatrix} \tag{60} $$

$$ {}^{E}_{2}\overline{\omega}^{E} = {}^{E}_{2}\overline{\omega}^{2} = \begin{bmatrix} 0 \\ 0 \\ \dot{\psi} \end{bmatrix} \tag{61} $$

Then,

$$ {}^{E}_{B}\overline{\omega}^{B} = {}^{1}_{B}\overline{\omega}^{B} + {}^{2}_{1}\overline{\omega}^{B} + {}^{E}_{2}\overline{\omega}^{B} \tag{62} $$

Expanding,

$$ \begin{bmatrix} p \\ q \\ r \end{bmatrix} = {}^{E}_{B}\overline{\omega}^{B} = {}^{1}_{B}\overline{\omega}^{B} + {}^{1}_{B}R^{T}_{x}\,{}^{2}_{1}\overline{\omega}^{B} + {}^{1}_{B}R^{T}_{x}\,{}^{2}_{1}R^{T}_{y}\,{}^{E}_{2}\overline{\omega}^{B} \tag{63} $$

Solving,

$$ \begin{bmatrix} p \\ q \\ r \end{bmatrix} = \begin{bmatrix} \dot{\phi} \\ 0 \\ 0 \end{bmatrix} + \begin{bmatrix} 1 & 0 & 0 \\ 0 & \cos\phi & \sin\phi \\ 0 & -\sin\phi & \cos\phi \end{bmatrix} \begin{bmatrix} 0 \\ \dot{\theta} \\ 0 \end{bmatrix} + \begin{bmatrix} 1 & 0 & 0 \\ 0 & \cos\phi & \sin\phi \\ 0 & -\sin\phi & \cos\phi \end{bmatrix} \begin{bmatrix} \cos\theta & 0 & -\sin\theta \\ 0 & 1 & 0 \\ \sin\theta & 0 & \cos\theta \end{bmatrix} \begin{bmatrix} 0 \\ 0 \\ \dot{\psi} \end{bmatrix} \tag{64} $$

$$ \begin{bmatrix} p \\ q \\ r \end{bmatrix} = \begin{bmatrix} \dot{\phi} - \dot{\psi}sin(\theta) \\ \dot{\theta}cos(\phi) + \dot{\psi}sin(\phi)cos(\theta) \\ -\dot{\theta}sin(\phi) + \dot{\psi}cos(\phi)cos(\theta) \end{bmatrix} = \begin{bmatrix} 1 & 0 & -sin(\theta) \\ 0 & cos(\phi) & sin(\phi)cos(\theta) \\ 0 & -sin(\phi) & cos(\phi)cos(\theta) \end{bmatrix} \begin{bmatrix} \dot{\phi} \\ \dot{\theta} \\ \dot{\psi} \end{bmatrix} \tag{65} $$

Such that,

$$ \mathrm{R}_2 = \begin{bmatrix} 1 & 0 & -sin(\theta) \\ 0 & cos(\phi) & sin(\phi)cos(\theta) \\ 0 & -sin(\phi) & cos(\phi)cos(\theta) \end{bmatrix} \tag{66} $$

As mentioned, R_2 converts generalized velocities from the earth frame to the body frame, and the inverse of this matrix, R_2^{-1}, does the opposite.

$$ \mathrm{R}_2^{-1} = \begin{bmatrix} 1 & sin(\phi)tan(\theta) & cos(\phi)tan(\theta) \\ 0 & cos(\phi) & -sin(\phi) \\ 0 & sin(\phi)/cos(\theta) & cos(\phi)/cos(\theta) \end{bmatrix} \tag{67} $$

B. KINEMATIC COEFFICIENTS

$$a_x = cos(\psi)sin(\theta)cos(\phi)z_g + sin(\phi)sin(\psi)z_g - cos(\psi)cos(\theta)x_g \tag{68}$$

$$a_y = -sin(\theta)cos(\phi)sin(\psi)z_g + cos(\psi)sin(\phi)z_g + cos(\theta)sin(\psi)x_g \tag{69}$$

$$a_z = cos(\phi)cos(\theta)z_g + sin(\theta)x_g \tag{70}$$

C. QUASI-VELOCITIES

For the presented airship, quasi-velocities $u_{1\to3}$ can be obtained by multiplying the transformation matrix R_1^{-1} by the derivatives of the generalized coordinates $q_{1\to3}$

$$u_1 = [cos(\psi)cos(\theta)]\dot{x} + [sin(\psi)cos(\theta)]\dot{y} - sin(\theta)\dot{z} \tag{71}$$

$$u_2 = a_1\dot{x} + a_2\dot{y} + a_3\dot{z} \tag{72}$$

$$u_3 = a_4\dot{x} + a_5\dot{y} + a_6\dot{z} \tag{73}$$

$$a_1 = cos(\psi)sin(\theta)sin(\phi) - sin(\psi)cos(\phi) \tag{74}$$

$$a_2 = sin(\psi)sin(\theta)sin(\phi) + cos(\psi)cos(\phi) \tag{75}$$

$$a_3 = sin(\phi)cos(\theta) \tag{76}$$

$$a_4 = cos(\psi)sin(\theta)cos(\phi) + sin(\psi)sin(\phi) \tag{77}$$

$$a_5 = sin(\psi)sin(\theta)cos(\phi) - cos(\psi)sin(\phi) \tag{78}$$

$$a_6 = cos(\phi)cos(\theta) \tag{79}$$

Similarly, quasi-velocities $u_{4\to6}$ are obtained by multiplying the transformation matrix R_2 by the time derivatives of $q_{4\to6}$.

$$u_4 = \dot{\phi} - sin(\theta)\,\dot{\psi} \tag{80}$$

$$u_5 = cos(\phi)\,\dot{\theta} + cos(\theta)sin(\phi)\,\dot{\psi} \tag{81}$$

$$u_6 = -sin(\phi)\,\dot{\theta} + cos(\theta)cos(\phi)\,\dot{\psi} \tag{82}$$

In this examination, the gondola's position is to remain constant as the work focuses on the lateral stability of the airship, where motion by the gondola is not required. Hence,

$$u_7 = \dot{S}_s = 0 \tag{83}$$